International Journal of Biodiversity and Conservation Vol. 2 (5), pp. 114-129, May, 2010
Available online http://www.academicjournals.org/ijbc
ISSN 2141 – 243x © 2010 Academic Journals

Full Length Research Paper

Variation of turbulent mixing parameters at the Egyptian Mediterranean coast

S. H. Sharaf El Din[1]*, F. M. Eid[1], N. N. Saad[2], K. A. Alam El Din[1], M. El Sharkawy[2]

[1]Oceanography Department, Faculty of Science, Alexandria University, Egypt.
[2]National Institute of Oceanography and Fisheries, Alexandria, Egypt.

Accepted 11 December, 2009

The analysis of the turbulent mixing structure is accomplished by the dynamical computations of the mixing parameters represented by: buoyancy frequency (N), viscous dissipation (ε), turbulent kinetic energy (E), Richardson number (Ri), Reynolds stress, diffusive salt flux (DSF), diffusive heat flux (DHF). In general the computations show that, the water column becomes more stable and less stratified at the deeper layers. Also, the dynamical processes of vertical turbulent mixing are stronger in the surface layers.

Key words: Mediterranean sea, turbulence mixing.

INTRODUCTION

The Egyptian Mediterranean Coast lies at the south east sector of the Levantine sub-basin, (Figure 1) from 25° 30' E to 34° E and extends northward to 33°N. Its water volume is about 224, 801, 55 km^3, and has a surface area of about 154,840 km^2.

Relatively, few efforts have been carried out to study the dynamical process of vertical turbulent mixing in front off the Egyptian Coast. Sharaf El-Din (1964) investigated the mixing processes in the North Sea and computed the Eddy coefficient of viscosity. Morcos and Hassan (1976) and Mohamed (1999) studied the dynamical process of mixing qualitatively by studying the existing different water masses. The mixing process and circulation pattern off Egyptian Mediterranean Coast was studied by El-Sharkawy (2007). The dynamics and mixing of the Eastern Mediterranean outflow in the Tyrrhenian basin was studied by Sparnocchia (1999). Nabil (2009) studied the turbulent vertical mixing parameters such as Richardson Number (Ri), Reynolds Stress (J_m) and Diffusive Salt Flux (J_s) at the central area of the Red Sea. Also, Johnson (1996); Rossa and Lueckb (2005); Munka and Wunschb (1998); Kobayashia et al. (2006); Hornea et al. (1996); MacPhee-Shaw (2006) and Yoshida and Oakey (1996) studies the vertical turbulent mixing using the numerical models at different parts of Oceans and Seas.

The aim of the present study is to investigate the variation of dynamical processes of vertical turbulent mixing water of the Egyptian Mediterranean Coast.

MATERIALS AND METHODS

The temperature and salinity data from 160 thousands stations through the Mediterranean Sea representing the time interval from the early 20th century till 2002; however, data only collected from 1970 - 2002 was used in this research. The measurements have been carried out by various instruments as CTD, MBT, XBT, and sampling bottles at the standard depths. This large data archive has been subject to sophisticated statistical modeling to render various types of error to the minimum. The average monthly climatologically data of 1° x 1° grid has been used in the proceeding calculations carried out in this work.

Four stations off the Egyptian Mediterranean Coast, Figure 1 named C12, C11, C10, and C1 were carried out to study the current field by the Eulerian method. Most of the hourly measurements of the current were provided by Arrays of Acoustic Doppler Current Profilers (ADCP); however, in some cases Recording Current Meters (RCM) was used.

Methods of analysis of turbulent mixing structure

Viscous dissipation (ε):

$$\varepsilon = K_m \left(\frac{\partial \left\| \vec{V} \right\|}{\partial z} \right)^2 \qquad 1$$

Where; ε is viscous dissipation of turbulent kinetic energy, K_m is the

*Corresponding author. E-mail: nabilelbatikhy@yahoo.com.

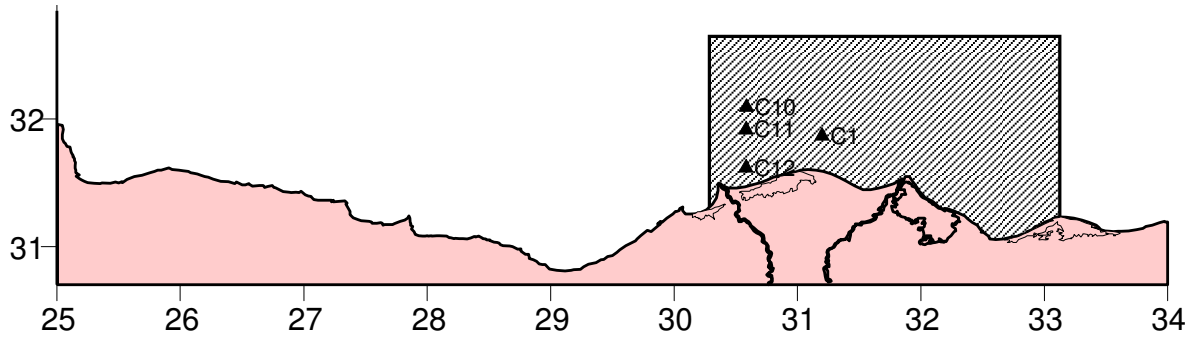

Figure 1. Area of study and location of current meter stations

Eddy Coefficient of viscosity; *V* is Northward velocity of current. Viscous Dissipation defines the rate of conversion of kinetic energy by viscosity (turbulent friction) to heat per unit mass (Proudman, 1953). This dynamical parameter is of negligible magnitude; however, it is a basic characteristic of mixing and the most important mixing parameter (Peters, 1999). The Eddy viscosity (K_m) is defined in terms of the molecular viscosity (μ), and density (ρ) by:

$$K_m = \mu / \rho \quad (2)$$

Turbulent kinetic energy (E) per unit mass (Pond and Pickard, 1983), which is a measure of turbulence

$$E = (U')^2 + (V')^2 \quad (3)$$

Where U' and V' are the deviation of eastward and northward velocity about its mean values respectively.

Brunt-vaisala frequency (N):

$$N = \sqrt{\frac{-g}{\rho}\frac{\partial \rho}{\partial z}} \quad (4)$$

Also, known as Buoyancy frequency. This is the natural frequency for the propagation of internal gravity waves (g) (Pond and Pickard, 1983), and is also a measure of dynamic stability.

Richardson number (Ri):

$$Ri = -\frac{N^2}{\left(\frac{\partial \|\vec{V}\|}{\partial z}\right)^2} \quad (5)$$

It is a non-dimensional indicator of the ensemble average flow state, but owing to the averaging, it is only loosely related to the dynamical instability and vertical turbulent mixing. However, values of *Ri* below the critical value (*Ri* = 0.25) Kelly (2005) and Robert (2005) indicate the occurrence of dynamical instability in the water column associated with strong processes of vertical turbulent mixing (Pond and Pickard, 1983).

Reynolds stress (J_m):

$$J_m = -\rho K_m \frac{\partial \|\vec{V}\|}{\partial z} \quad (6)$$

Which defines the vertical turbulent flux of momentum (Peters, 1999)?

Eddy diffusivity (K_s):

$$K_s = 0.2 \times \frac{\varepsilon}{N^2} \quad (7)$$

This defines the turbulent exchange coefficient of Salt (Peters, 1999).

Diffusive salt flux (J_s):

$$J_s = -10^{-3} \rho K_s \left(\frac{\partial S}{\partial z}\right) \quad (8)$$

This defines the vertical turbulent transport of salt (Peters, 1999).

Diffusive heat flux (J_h):

$$J_h = -\rho C_p K_h \left(\frac{\partial T}{\partial z}\right) \quad (9)$$

This defines the vertical turbulent transport of heat (Molinari et al., 1986), where the specific heat C_p=3.94 k j / kg c°, and the coefficient of heat diffusivity $K_h = 1 \times 10^{-4}$ m^{-2}s^{-1}

RESULTS AND DISCUSSION

The dynamical computations for turbulence mixing parameters are carried out for the four stations C12, C11, C10 and C1 at three levels: near surface, intermediate depth, and near bottom. The depth of the three levels selected

Table 1. The three levels depths selected through the four casts of current stations.

	C12 m	C11 m	C10 m	C1 m
near surface	3	14	42	8
intermediate depth	10	46	170	34
near bottom	18	94	298	58

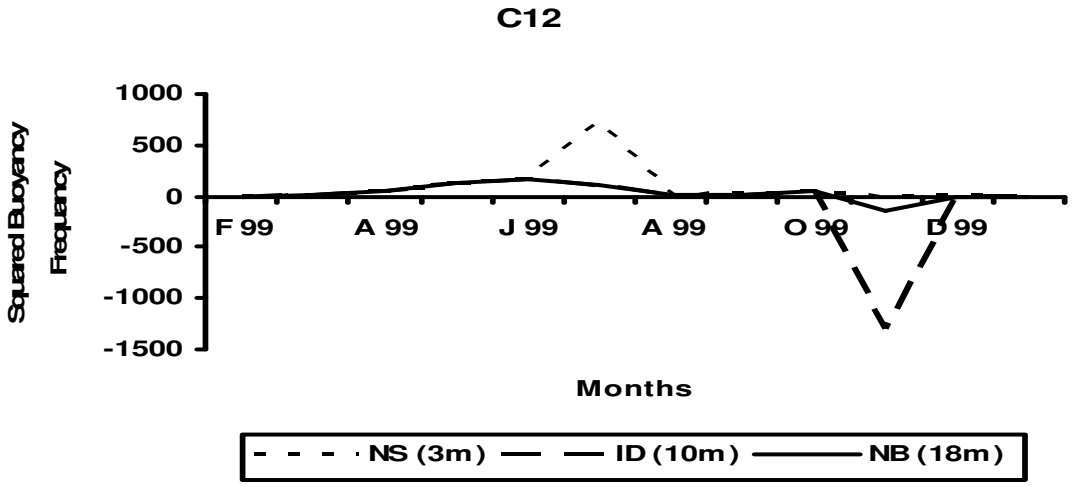

Figure 2a. Squared buoyancy frequency (10^{-6} s^{-2}) at stations C12.

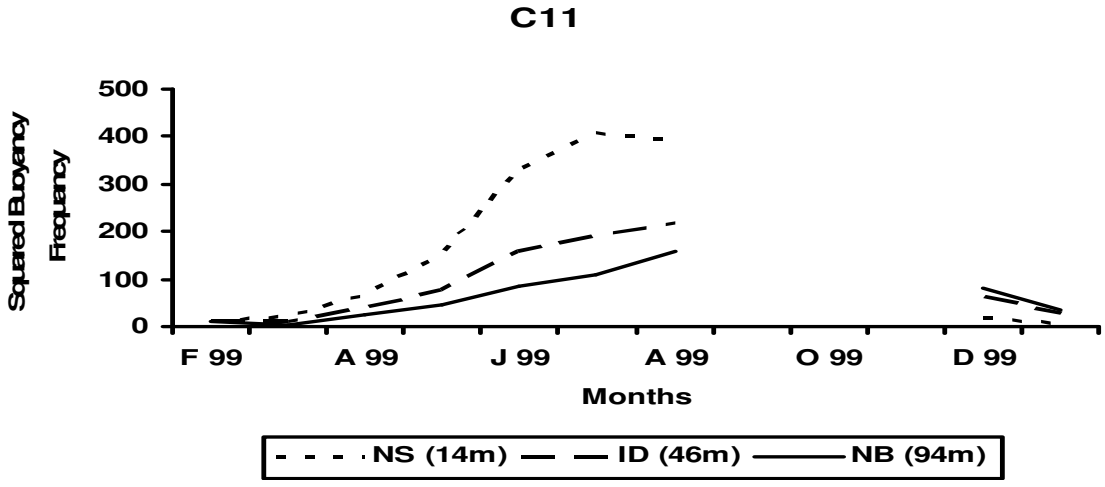

Figure 2b. Squared buoyancy frequency (10^{-6} s^{-2}) at stations C11.

through the four stations was tabulated in Table 1.

Brunt-Vaisala frequency or the buoyancy frequency (*N*)

As the static stability is positive for stable conditions and zero or negative for unstable conditions, the result values of N^2 at all stations attained positive values during the whole year except at station C12, it had negative values during the period from November to February. Theses negative values, appeared during the cold period, related to occurrence of dynamic instability in the water column associated with strong processes of vertical turbulent mixing, Figure (2a). At C12, values of N^2 vary from -1.28 × 10^{-3} s^{-2} at 10 m (intermediate depth) during November to 7.19 × 10^{-4} s^{-2} at 3 m (near surface) during July with an annual vertical average value -6.64 × 10^{-5} s^{-2}. The water column was stable at station C11 Figure (2b). Values of N^2 vary from 4.98 × 10^{-6} s^{-2} during March at 94 m (near bottom) to 410 × 10^{-6} s^{-2} during July at 14 m (near surface) with an annual vertical average value 1.12 × 10^{-4} s^{-2}.

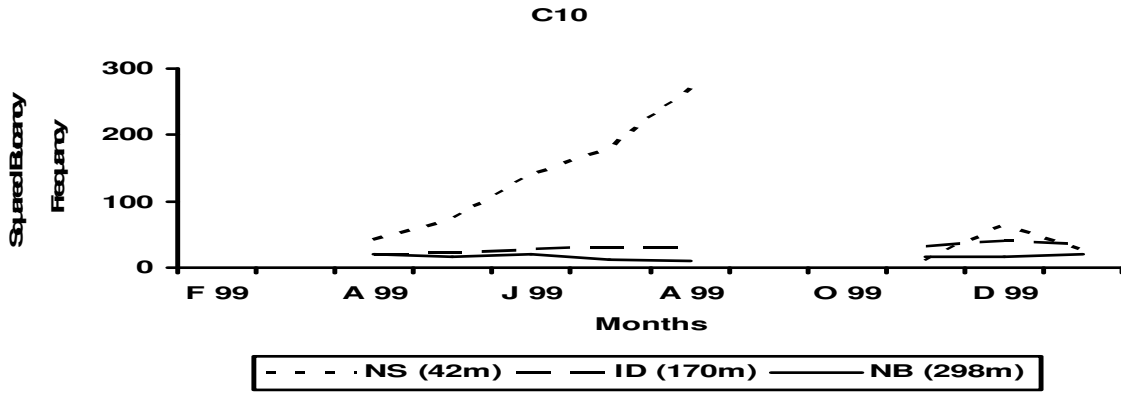

Figure 2c. Squared buoyancy frequency (10^{-6} s^{-2}) at station C10.

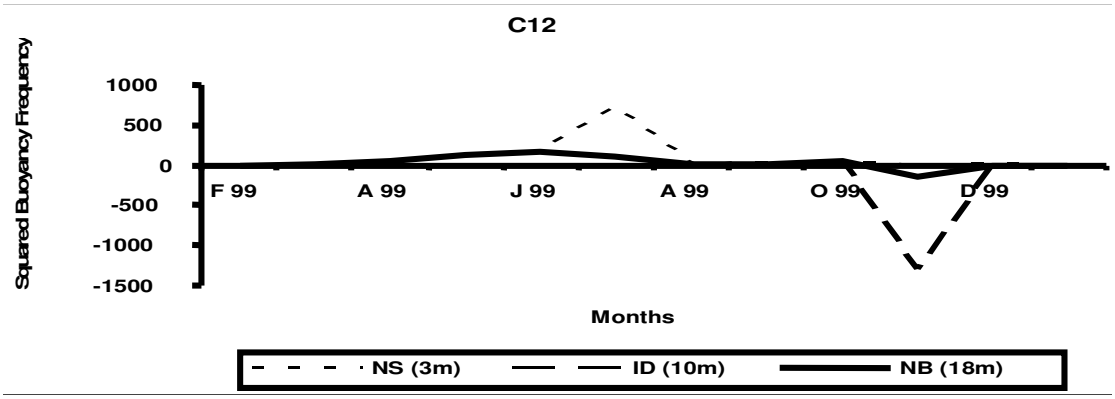

Figure 2d. Squared buoyancy frequency (10^{-6} s^{-2}) at station C1.

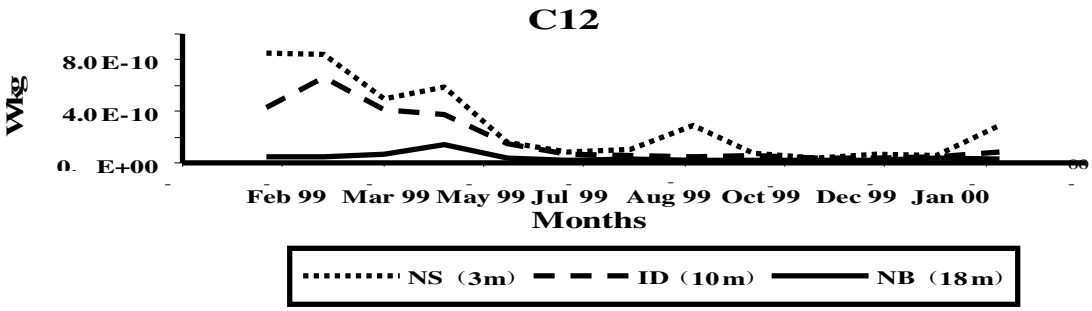

Figure 3a. Dissipated energy (w/kg) at station C12.

At station C10, Figure (2c), the water column also showed dynamic stability as values of N^2 vary from 9.59 × 10^{-6} s^{-2} during November at 42 m (near surface) to 2.66 × 10^{-4} s^{-2} during August at 42 m also with an annual vertical average value 4.58 × 10^{-5} s^{-2}. The water column was unstable (N^2 negative) at station C1, Figure (2d) during November and December, and values N^2 varies from -5.47 × 10^{-6} s^{-2} during December at 8 m (near surface) to 3.72 × 10^{-4} s^{-2} during July at 34 m (intermediate depth) with an annual vertical average value 9.53 × 10^{-5} s^{-2}.

The viscous dissipation

At station C12, Figure (3a), ε attained its greatest values during February which reached 8.52 × 10^{-10} W/kg at 3 m (near surface). The minimum value of ε was 1.68 × 10^{-11} W/kg attained during November at 18 m (near bottom), and the annual vertical average value was 1.77 × 10^{-10}

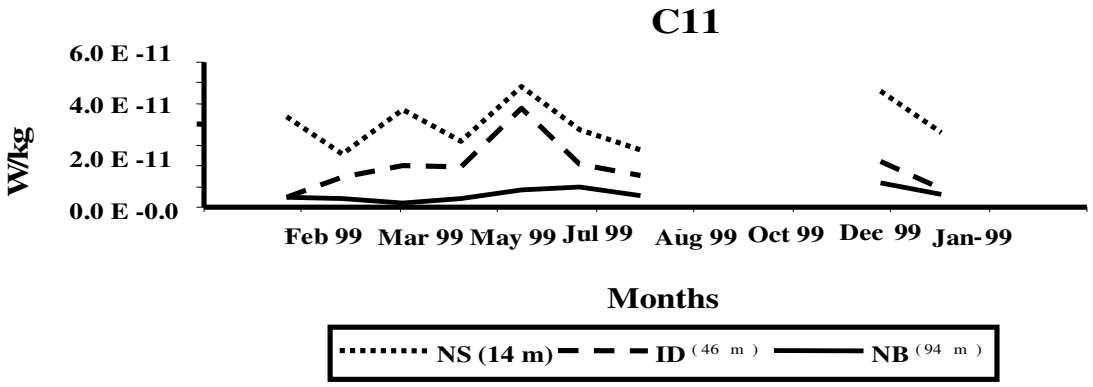

Figure 3b. Dissipated energy (w/kg) at station C11.

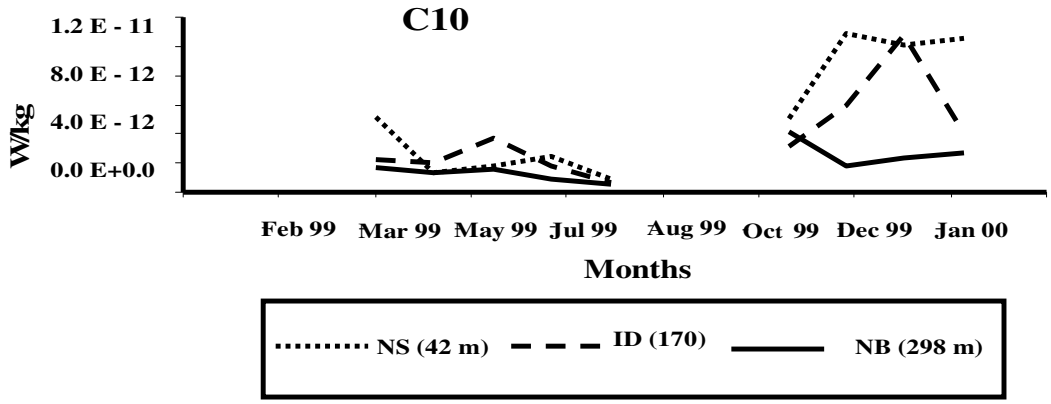

Figure 3c. Dissipated energy (w/kg) at station C10.

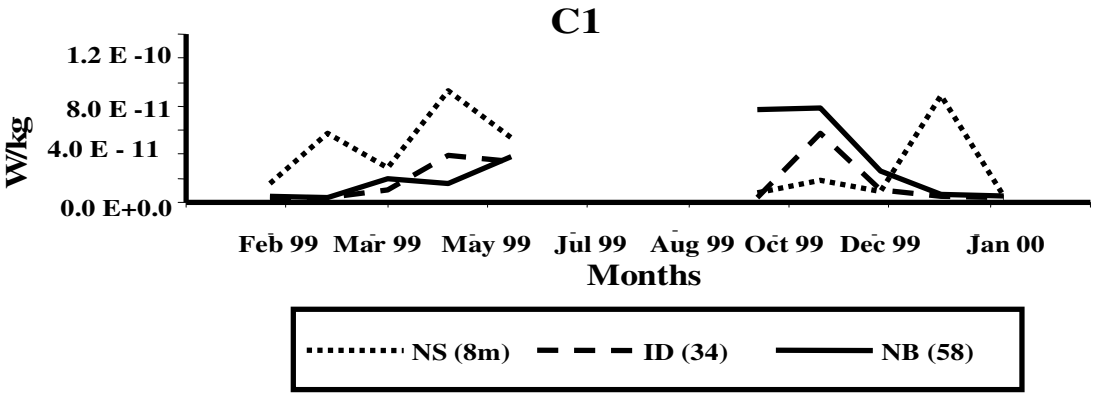

Figure 3d. Dissipated energy (w/kg) at station C1.

W/kg.

For the deeper stations C11, C10, and C1, (Figures 3b, c and d), it can be noticed that ε had relatively smaller magnitudes. For instance, at station C11, values ε range from 2.04×10^{-12} W/kg during April at 94 m (near bottom) to 5.81×10^{-11} W/kg during June at 14 m (near surface) with an annual vertical average value 2.18×10^{-11} W/kg. The viscous dissipated energy, at the deep station C10, was the weakest among the four stations as ε ranged from 5.76×10^{-13} W/kg during August at 298 m (near bottom) to 1.09×10^{-11} W/kg during December at 42 m (near surface), with an annual vertical average value

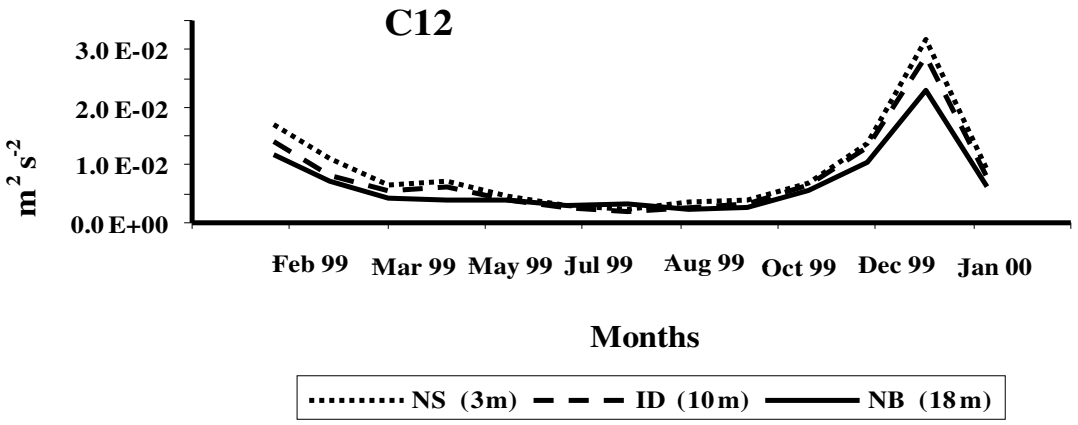

Figure 4a. Turbulent kinetic energy (m^2s^{-2}) at station C12.

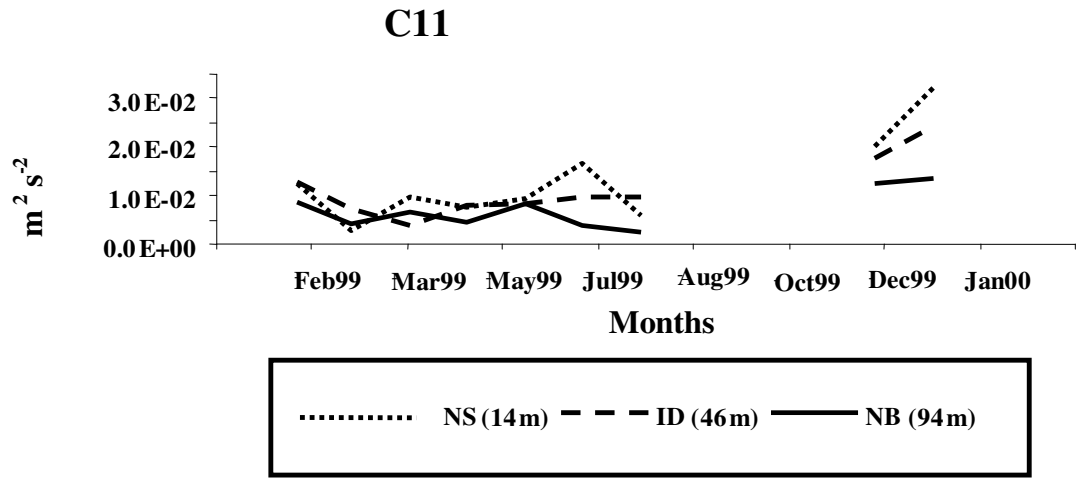

Figure 4b. Turbulent kinetic energy (m^2s^{-2}) at station C11.

3.69×10^{-12} W/kg.

The dissipation of turbulent kinetic energy by viscosity was relatively higher at station C1. Values of ε range from 3.4×10^{-12} W/kg during February at 34 m (intermediate depth) to 1.23×10^{-10} W/kg during August at 8 m (near surface) with an annual vertical average value 3.21×10^{-11} W/kg. It can be noticed that the maximum viscous dissipation always occur near the surface, that is, ε decreases with depth. This showed that the processes of vertical turbulent mixing were stronger in the upper layers.

The turbulent kinetic energy

Figures 4a revealed that at station C12, *E* ranged from 2.05×10^{-3} m^2s^{-2} at 10 m (intermediate depth) during August to 3.18×10^{-2} m^2s^{-2}at 3 m (near surface) during January, with an annual vertical average value 8.03×10^{-3} m^2s^{-2}. The behavior of *E* at station C11 was quite analogous; (Figure 4b), as *E* ranges from 2.36×10^{-3} m^2s^{-2} at 94 m (near bottom) during August to 3.22×10^{-2} m^2s^{-2}at 14 m (near surface) during January, with an annual vertical average value 1.04×10^{-2} m^2s^{-2}.

The computations revealed that *E* decreased significantly with depth. This can be seen from the distribution of *E* at the deep station C10, (Figure 4c), where *E* ranges from 8.19×10^{-4} m^2s^{-2} at 298 m (near bottom) during August to 8.26×10^{-2} m^2s^{-2}at 42 m (near surface) during December, with an annual vertical average value 1.17×10^{-2} m^2s^{-2}. At the station C1 (Figure 4d), *E* ranged from 2.14×10^{-3} m^2s^{-2} at 58 m (near bottom) during August to 3.47×10^{-2} m^2s^{-2}at 8 m (near surface) during December, with an annual vertical average value 8.62×10^{-3} m^2s^{-2}.

This temporal distribution of *E* shows that turbulence was stronger near the surface and decrease with depth, that is, the motion of water was more laminar at deeper layers. The minimum values of *E* were attained during August while the maximum ones were attained during December and January, that is, turbulence is weaker in

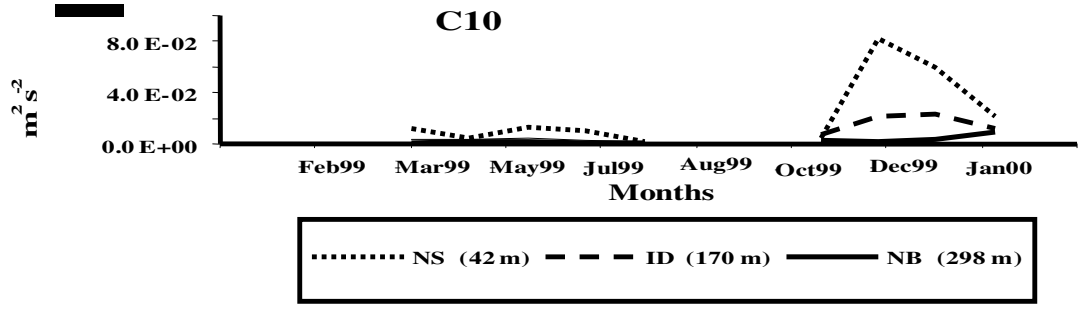

Figure 4c. Turbulent kinetic energy (m^2s^{-2}) at station C10.

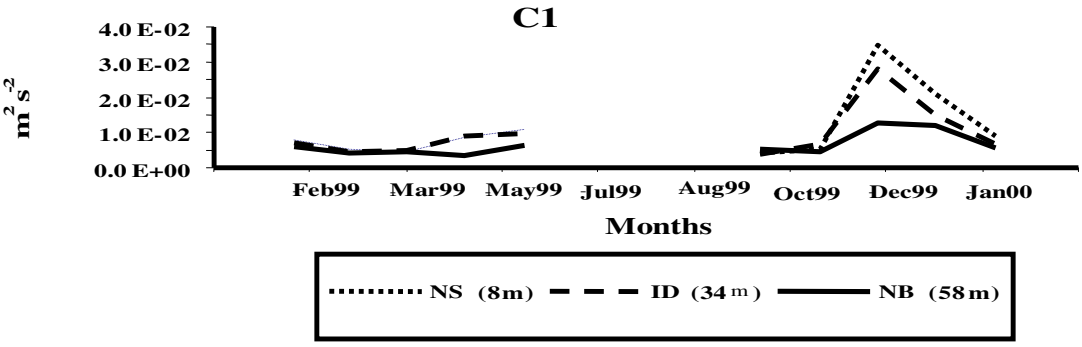

Figure 4d. Turbulent kinetic energy (m^2s^{-2}) at station C1.

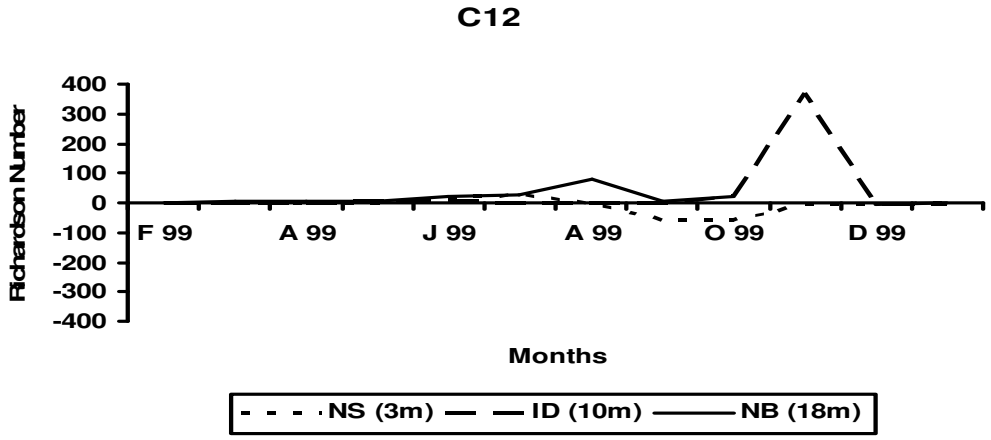

Figure 5a. Richardson number at station C12.

summer and stronger in winter.

The Richardson number *Ri*

From Figure (5a), the distribution of *Ri* at the shallow station C12 is characterized by possessing a maximum value of 367, attained during November at 10 m (near surface), with an annual vertical average value of 2.29. Negative values of *Ri* remarked at 3 m between august and December at C12 resulted from negative values of N^2 which indicated unstable density gradients with active convective overturning. Under such circumstances, *N* does not have an accepted physical meaning and the magnitude of negative *Ri* is not generally of interest.

Stations C11 and C10 (Figures 5b and c) are charac-

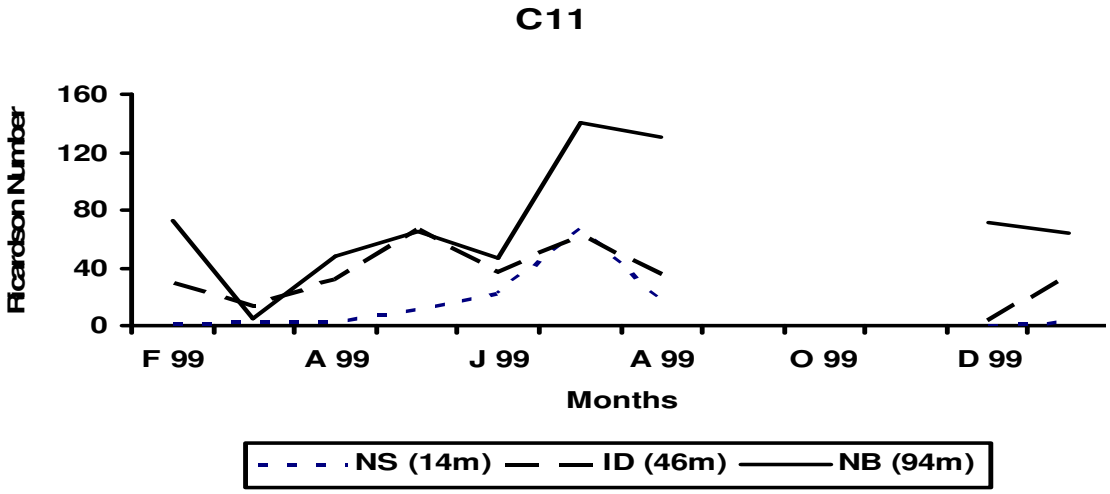

Figure 5b. Richardson number at station C11.

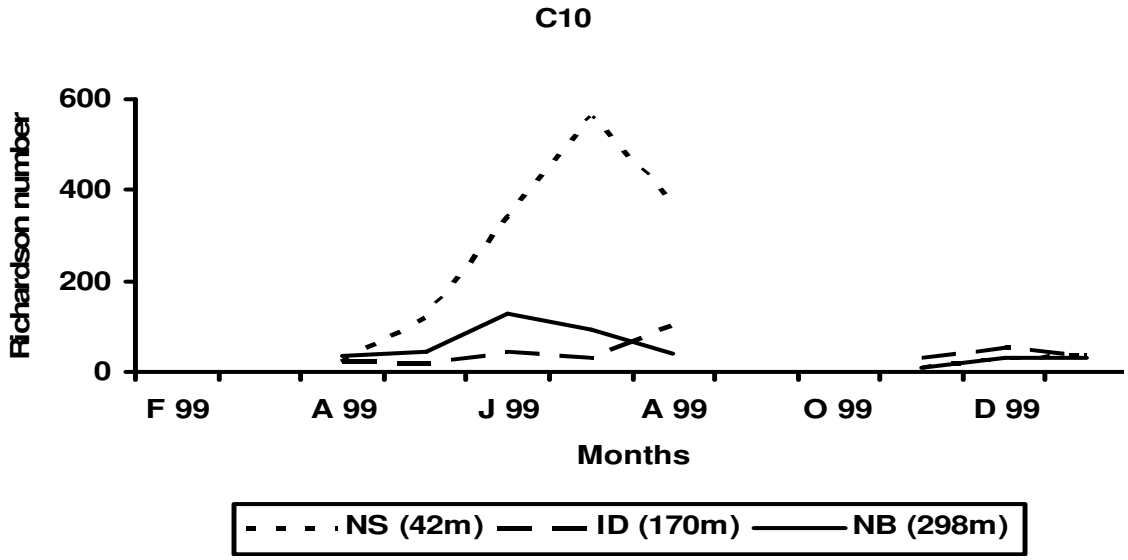

Figure 5c. Richardson number at station C10.

terized by possessing only positive values of *Ri*. Values of this dynamical parameter vary at station C11 from 0.54, attained during December at 14 m (near surface) to 140, attained during July at 94 m (near bottom) with an annual vertical average value 41.4. At the deep station C10, *Ri* varies from 9.30 attained during November at 42 m (near surface) to 558 attained during July at 42 m also with an annual vertical average value 8.51. A very small negative value of *Ri*, occurred again at station C1, (Figure 5d) during the cold months. *Ri* varied from 0.07 during May at 34 m (intermediate) to 228, attained during October at 34 m (intermediate) with an annual vertical average value 29.4. The behavior of *Ri*, on contrary to that of N^2, ε, *E*, shows no time or spatial dependence.

The Reynolds stress J_m

At the shallow station C12, J_m varies from -1.6×10^{-6} Pa, attained during August at 18 m (near bottom) to 8.07×10^{-6} Pa, attained during March at 3 m (near surface), with an annual vertical average value 2.29×10^{-6} Pa. Hereinafter, The negative sign indicates that the vertical transport was directed upwards and vice versa, (Figures 6a). The maximum upward Reynolds stress, at the station C11, (Figure 6b) occurred during January at 14 m (near surface) with magnitude -1.1×10^{-6} Pa, the maximum downward momentum flux occurs during March at 14 m also with a magnitude 3.8×10^{-6} Pa, while the annual vertical average value of J_m was.72×10^{-7} Pa.

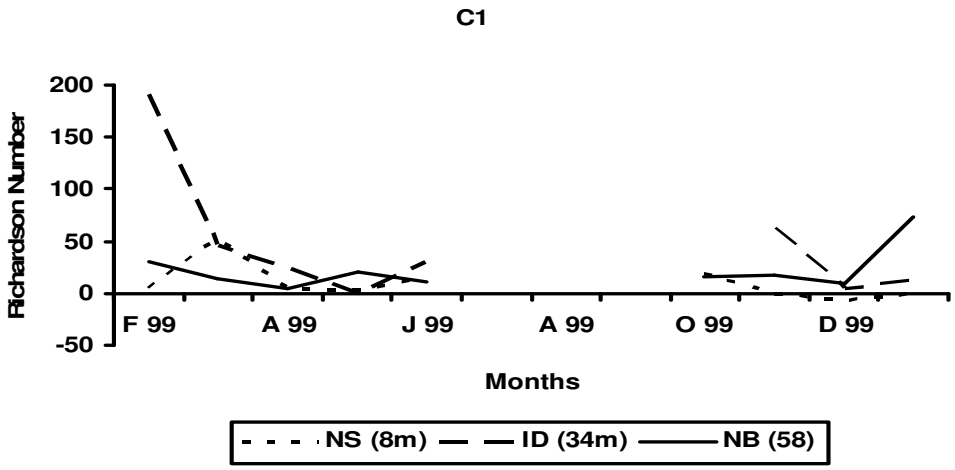

Figure 5d. Richardson number at station C1.

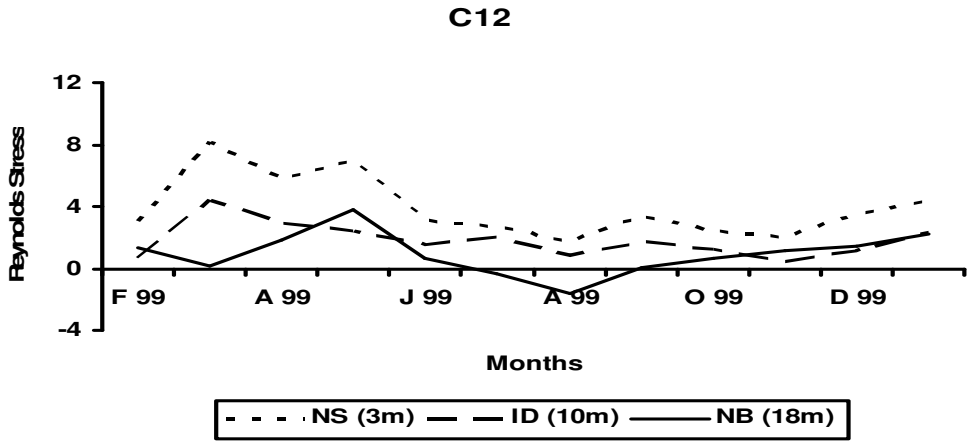

Figure 6a. Reynold's Stress (10^{-6} Pa) at station C12.

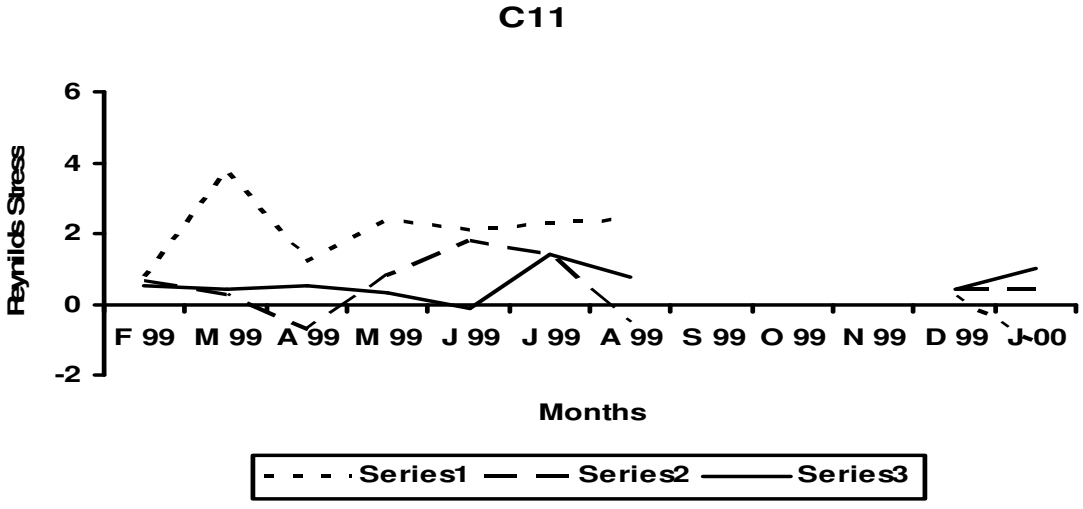

Figure 6b. Reynold's Stress (10^{-6} Pa) at station C11.

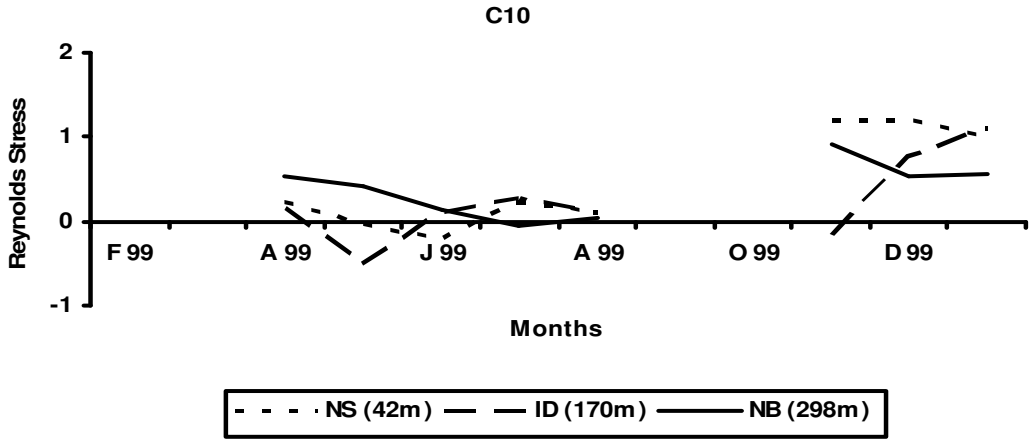

Figure 6c. Reynold's Stress (10^{-6} Pa) at station C10.

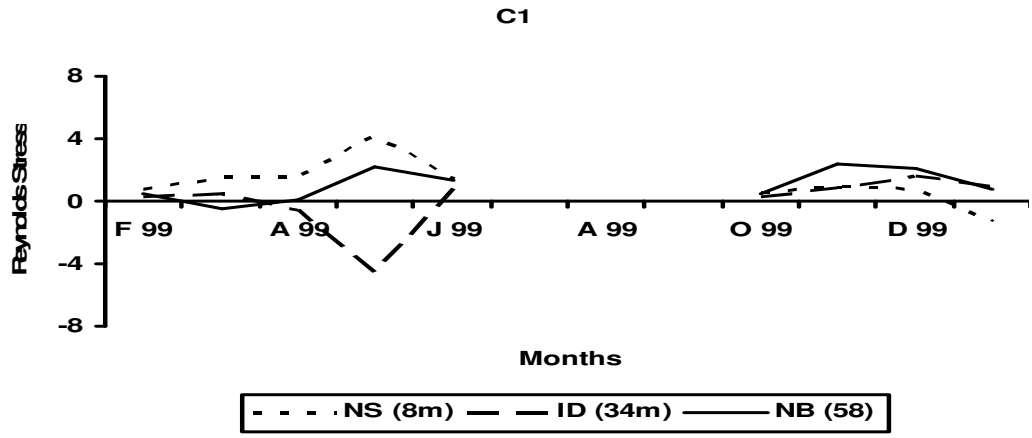

Figure 6d. Reynold's Stress (10^{-6} Pa) at station C1

Relatively weaker momentum fluxes occurred at the deep station C10, (Figure 6c) as J_m varied from -4.99 × 10^{-7} Pa, attained during May at 170 m (intermediate depth) to 1.2 × 10^{-6} Pa attained during November at 42 m (near surface), with an annual vertical average value 4.09 × 10^{-7} Pa. For station C1, (Figure 6d), a maximum upward momentum flux occurred during January at 8 m (near surface) with magnitude -1.25 × 10^{-6} Pa, the maximum downward momentum stress occurred during August at 58 m (near bottom) with a magnitude of4.39 × 10^{-6} Pa, while the annual vertical average value was 1.13 × 10^{-6} Pa.

The Eddy diffusivity

Figure 7a, showed the dynamical computations of Eddy diffusivity. At the four stations, the magnitude of K_s decreased relatively with depth. The temporal distribution of K_s at the shallow station C12 showed that K_s had maximum magnitude of 2.0 × 10^{-6} m^2s^{-1}, attained during April at 3 m (near surface), and a minimum magnitude of -1.0 × 10^{-6} m^2s^{-1} attained during December at 3m Also, with an annual vertical average value -0.3 × 10^{-6} m^2s^{-1}. Negative values of K_s result from negative values of N^2 which were associated with dynamical instability.

The minimum magnitude of K_s at the station C11, (Figure 7b), was 0.01 × 10^{-6} m^2s^{-1}, attained during August at 94 m (near bottom), while the maximum magnitude was 1.22 × 10^{-6} m^2s^{-1} attained during January at 14 m (near surface) with an annual vertical average value 1.46× 10^{-7} m^2s^{-1}. Magnitudes of K_s were relatively weaker at the deep station C10, Figure (7c) as the minimum magnitude is 7.12 × 10^{-10} m^2s^{-1} during August at 42 m (near surface), the maximum magnitude is 0.07 × 10^{-6} m^2s^{-1} attained during January at 42 m (near surface) with an annual vertical average value of 7.14 × 10^{-8} m^2s^{-1}. At station C1, Figure (7d) the minimum magnitude of K_s is-2.7 × $10^{-6}$$m^2s^{-1}$ attained during May at 34 m (near surface), the maximum magnitude was 2.8 × 10^{-6} m^2s^{-1} attained

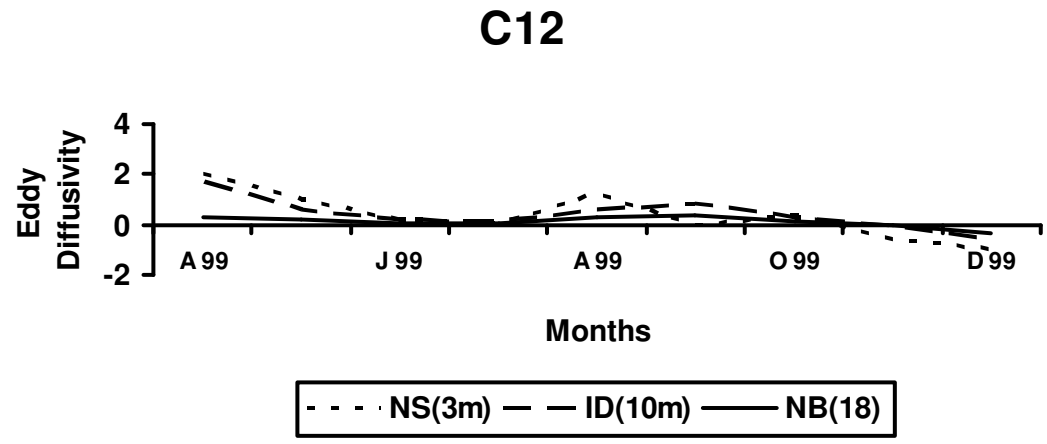

Figure 7a. Eddy diffusivity (10^{-6} m^2 s^{-1}) at station C12.

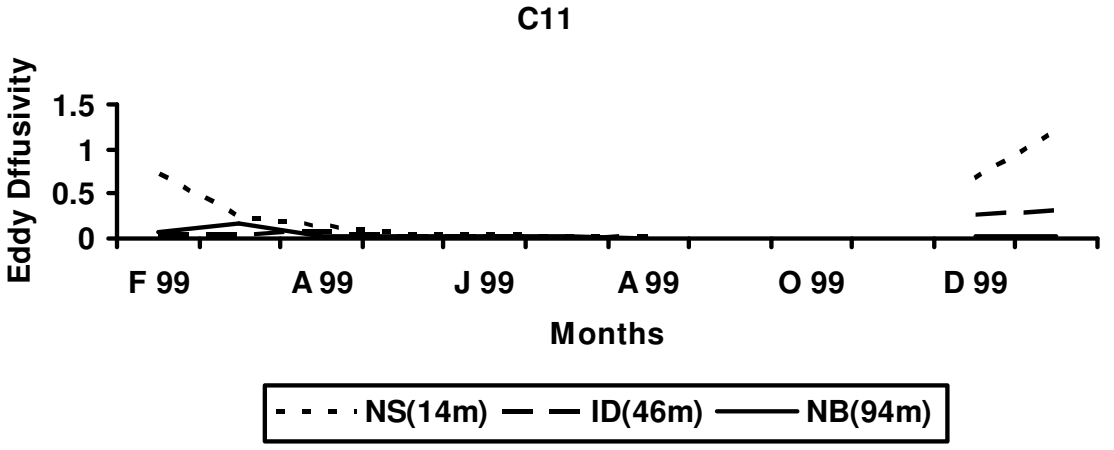

Figure 7b. Eddy diffusivity (10^{-6} m^2 s^{-1}) at station C11.

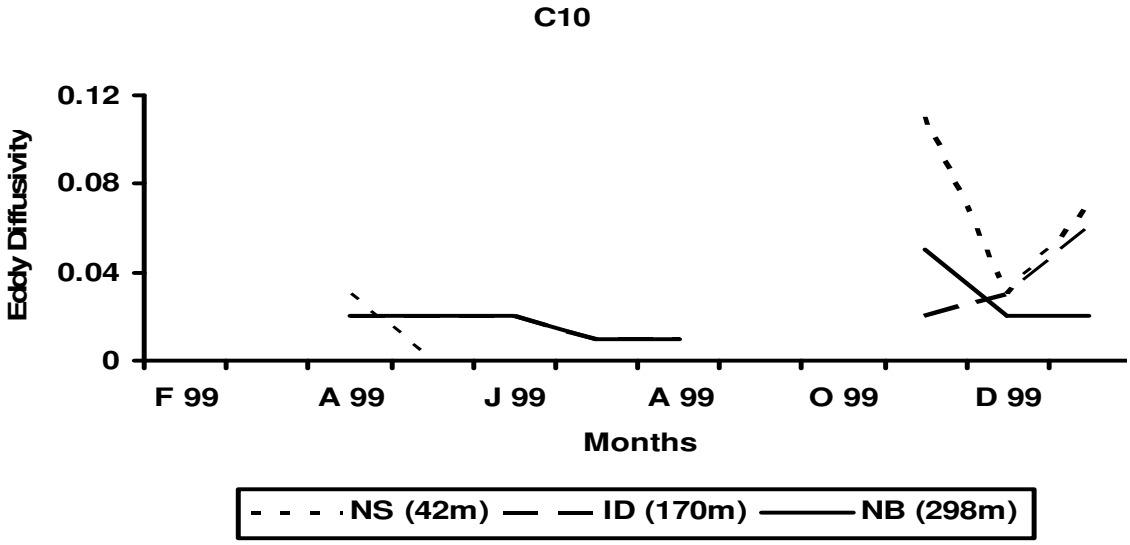

Figure 7c. Eddy diffusivity (10^{-6} m^2 s^{-1}) at station C10.

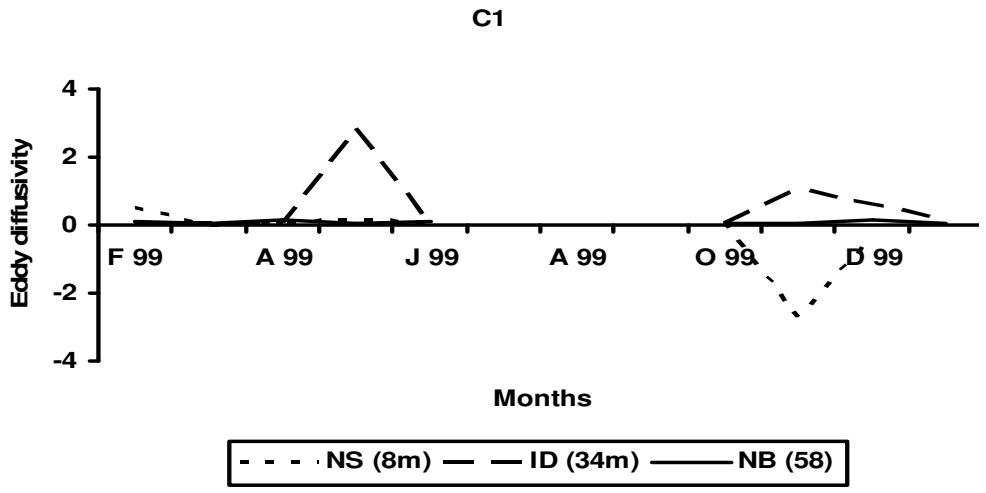

Figure 7d. Eddy diffusivity (10^{-6} m^2 s^{-1}) at station C1.

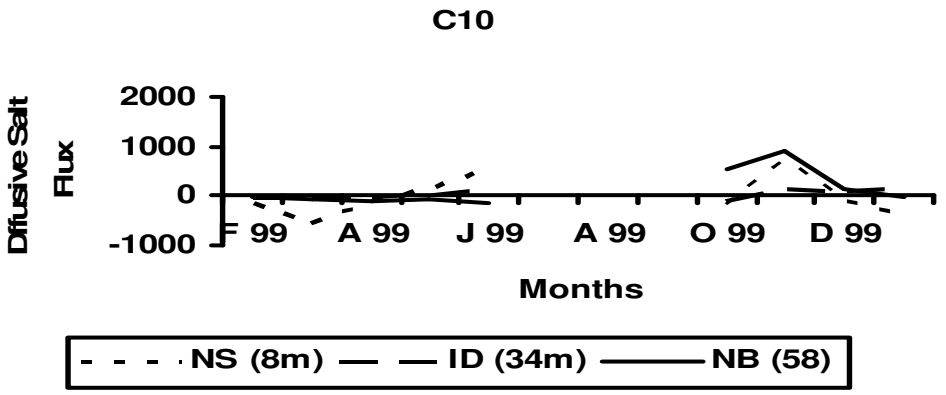

Figure 8a. Diffusive salt flux (10^{-12} kg m^2 s^{-1}) at station C10.

during January at 8 m (intermediate), while the annual vertical average value -7.04 × 10^{-7} m^2s^{-1}.

The diffusive salt flux

The numerical results showed that the distribution of J_s was analogous to that of K_s as both distributions reveal that the magnitudes of these two mixing parameters increased significantly during winter, and also decreased relatively with depth.

From Figure 8a the shallow station C12, J_s varied from a minimum of -2.49 × 10^{-8} kg $m^{-2}s^{-1}$ attained during March at 3 m flowing upwards to a maximum of 2.78 × 10^{-9} kg $m^{-2}s^{-1}$ attained during February, at 3 m also flowing downwards, with an annual vertical average value of 1.49 × 10^{-8} kg $m^{-2}s^{-1}$. Magnitudes of DSF at this shallow station C12 (21 m) are significantly greater than other stations due to the existence of strong vertical gradient of salt in the water column. Strong vertical gradients of salt could result from evaporation which had greater effect on the upper layer or could result from near boundary currents. Yoshida et al (1999) found that diffusivity and mixing processes were stronger near the bottom of the shallow Georges Bank (Canada) and that mixing was maximum when the flow is strongest.

For the deeper stations C11, C10, and C1, Figure (8b) it can be noticed that J_s has smaller magnitudes. For instance, at station C11, J_s ranged from a minimum of -1.98 × 10^{-10} kg $m^{-2}s^{-1}$ attained during February at 14 m directed upwards to a maximum of 1.26 × 10^{-9} kg $m^{-2}s^{-1}$ attained during January at 14 m also directed downwards, with an annual vertical average value 8.87 × 10^{-11} kg $m^{-2}s^{-1}$. The vertical diffusive salt flux at station C10, (Figure 8c) ranged from a minimum of -66 × 10^{-12} kg $m^{-2}s^{-1}$ attained during December at 170 m to a maximum of 1.8 × 10^{-10} kg $m^{-2}s^{-1}$ attained during November at 42 m, with an annual vertical average value of 4.73 × 10^{-11} kg $m^{-2}s^{-1}$. At station C1, (Figure 8d) J_s ranges from a minimum of -5.34 × 10^{-10} kg $m^{-2}s^{-1}$ attained during March

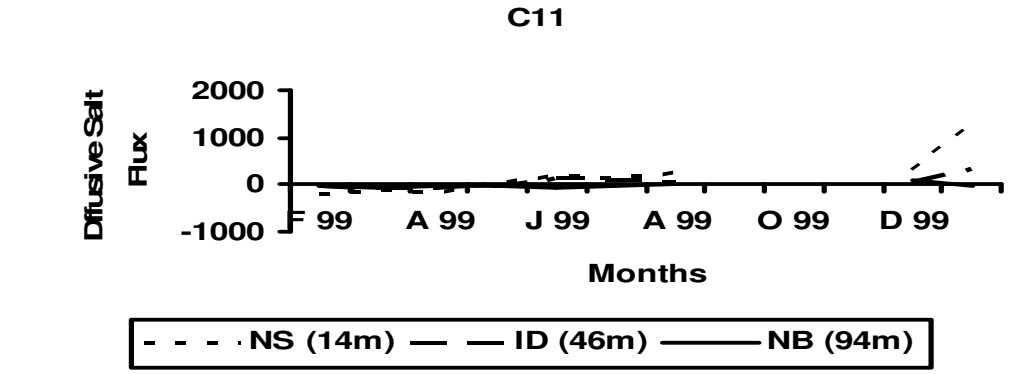

Figure 8b. Diffusive salt flux (10^{-12} kg m^2 s^{-1}) at station C11.

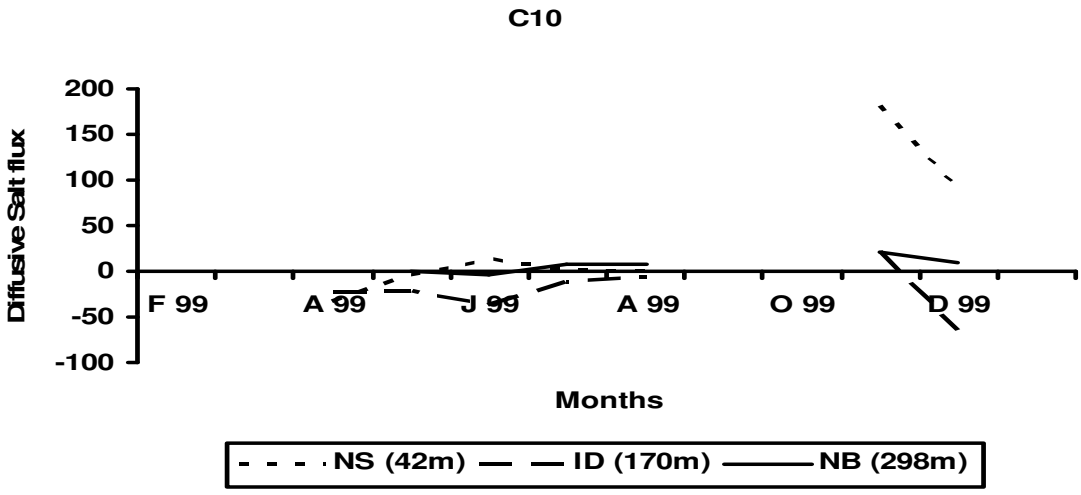

Figure 8c. Diffusive salt flux (10^{-12} kg m^2 s^{-1}) at station C10.

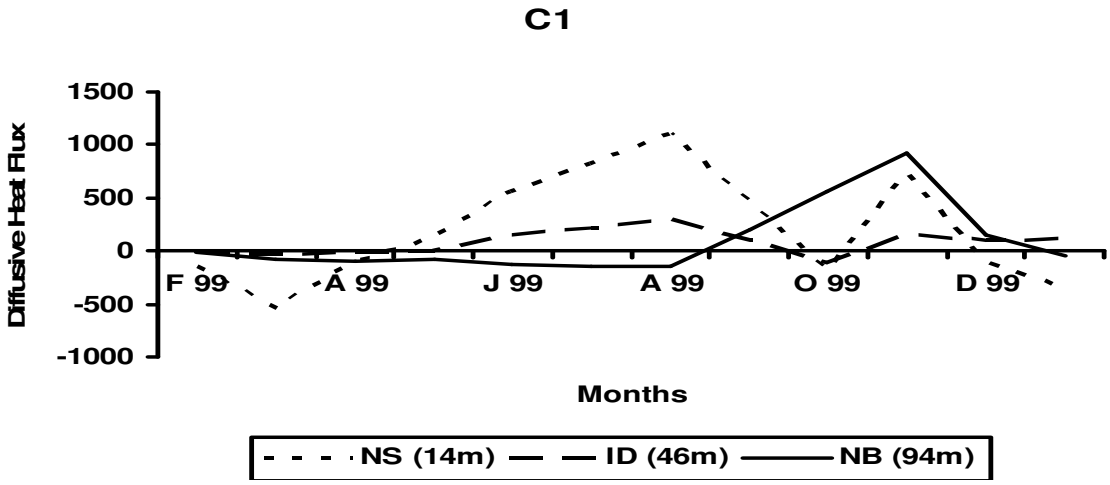

Figure 8d. Diffusive salt flux (10^{-12} kg m^2 s^{-1}) at station C1.

at 8 m to a maximum of 1.07×10^{-9} kg $m^{-2}s^{-1}$ attained during August at 8 m also with an annual vertical average value 8.18×10^{-11} kg $m^{-2}s^{-1}$.

The diffusive heat flux

The temporal distribution of DHF at station C12, (Figure 9a)

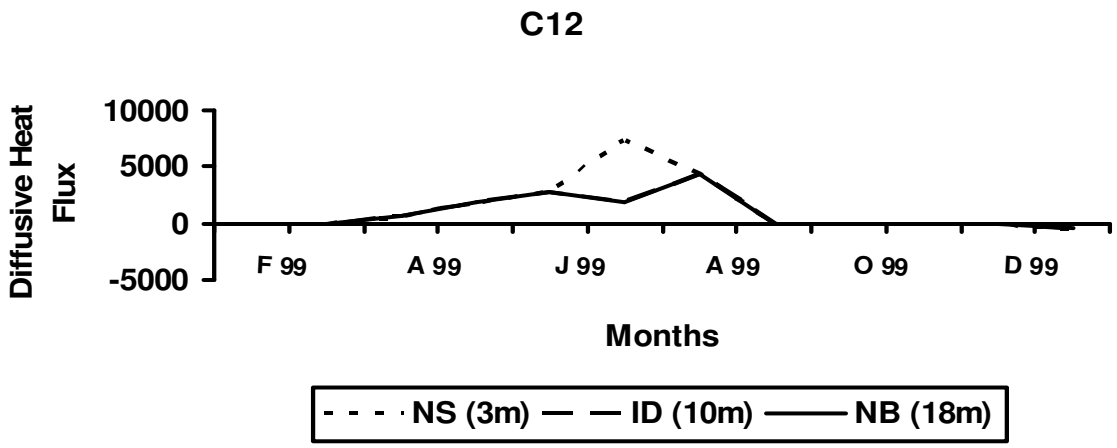

Figure 9a. Diffusive heat flux (10^{-6} j m^2 s^{-1}) at station C12.

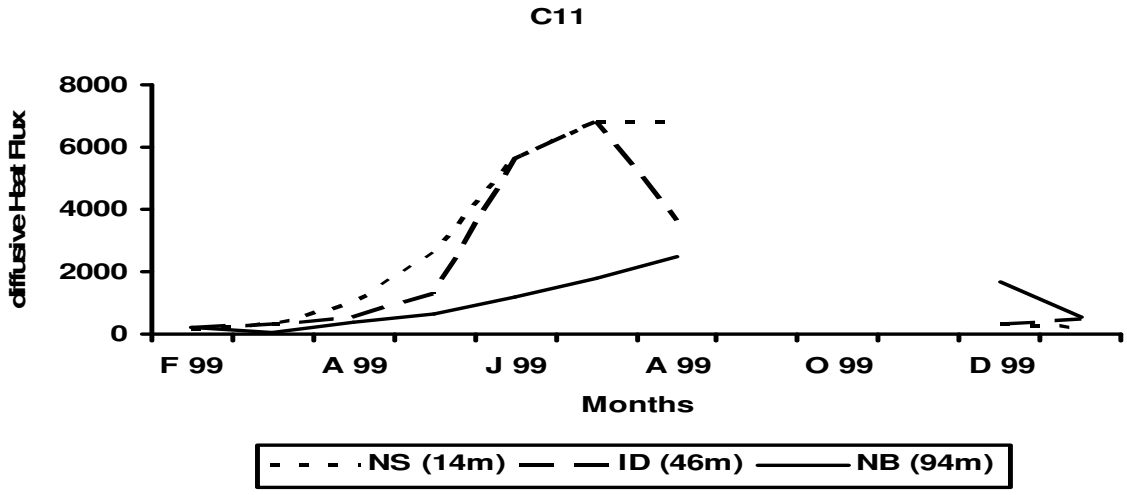

Figure 9b. Diffusive heat flux (10^{-6} j m^2 s^{-1}) at station C11.

had a minimum of -3.38 × 10^{-4} j $m^{-2}s^{-1}$, attained during January at 3 m which mean losses of temperature from the sea, and a maximum value of 7.27 × 10^{-3} j $m^{-2}s^{-1}$ attained during July at 3 m also, (that is, sea water gained temperature from surrounding environments) with an annual vertical average value of 9.32 × 10^{-4} j $m^{-2}s^{-1}$..

Only downward fluxes of heat occur at station C11, Figure (9b) as J_h varied from a minimum of 4.87 × 10^{-5} j $m^{-2}s^{-1}$ attained during March at 94 m to a maximum of 6.83 × 10^{-3} j $m^{-2}s^{-1}$ attained during August at 14 m, with an annual vertical average value of 2.05 × 10^{-3} j $m^{-2}s^{-1}$. The vertical turbulent transport of heat at station C10, Figure (9c) ranges from a minimum of 240 × 10^{-6} j $m^{-2}s^{-1}$ attained during April at 170 m (intermediate), to a maximum of 4.24 × 10^{-3} j $m^{-2}s^{-1}$ attained during August at 42 m, with an annual vertical average value of 8.31 × 10^{-4} j $m^{-2}s^{-1}$.

The temporal behavior of DHF at station C1, (Figure 9d) was analogous to other three stations as values of J_h ranged from a minimum of -7.1×10^{-3} j $m^{-2}s^{-1}$ attained during November at 34 m (intermediate depth) to maximum of 6.59 × 10^{-3} j $m^{-2}s^{-1}$ at 34 m attained during August, with an annual vertical average of 1.16 × 10^{-3} j $m^{-2}s^{-1}$. Thus, the temporal distribution of DHF, similarly to the buoyancy frequency, posse's maximum values during summer (July and August) which indicated that the two mixing parameters were related strongly to the heating by solar radiation. Also, the DHF generally decreased with depth, and was generally positive, that is, the heat flux was directed downwards.

Summary and Conclusion

The dynamical computations for turbulence mixing parameters are carried out for the four stations C12, C11, C10

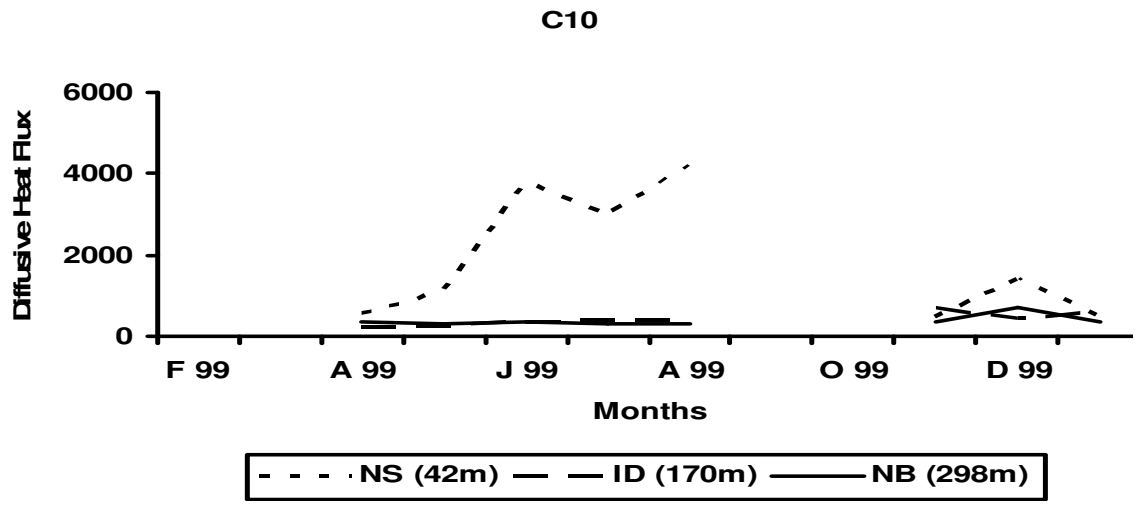

Figure 9c. Diffusive heat flux (10^{-6} j m^2 s^{-1}) at station C10.

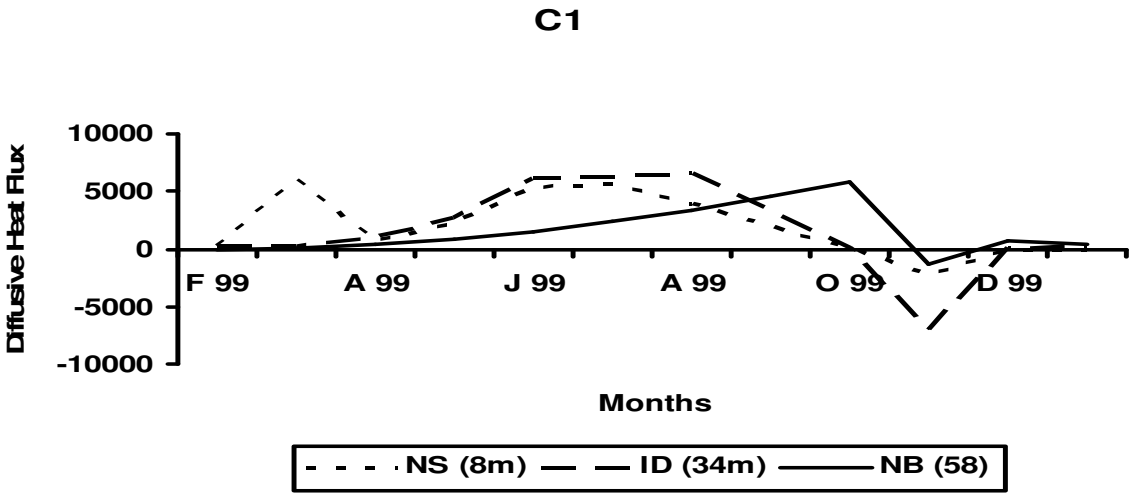

Figure 9d. Diffusive heat flux (10^{-6} j m^2 s^{-1}) at station C1.

and C1 at three levels: near surface, intermediate depth and near bottom In general, it is noticed that the greatest values of N^2 are attained during summer, in coincidence with the solar radiation, and the lowest values occur during autumn and winter. Also the absolute value of N^2 decreases with depth indicating that lower layers are less stratified and more homogenous. It can be noticed that the maximum viscous dissipation always occur near the surface, that is, ε decreases with depth. This shows that the processes of vertical turbulent mixing are stronger in the upper layers. This temporal distribution of E shows that turbulence is stronger near the surface and decrease with depth, that is, the motion of water is more laminar at deeper layers. The minimum values of E are attained during August while the maximum ones are attained during December and January, that is, turbulence is weaker in summer and stronger in winter. The behavior of Ri, on contrary to that of N^2, ε, E, shows no time or spatial dependence. The maximum upward Reynolds stress J_m is observed near surface during winter season while downward momentum flux occurs at near bottom during summer season. The dynamical computations of the magnitude K_s at the four stations decrease relatively with depth. The temporal distribution of DHF, similarly to the buoyancy frequency, posse's maximum values during summer (July and August) which indicate that the two mixing parameters are related strongly to the heating by solar radiation. Also, the DHF generally decreases with depth, and is generally positive, that is, the heat flux is directed downwards.

REFERENCES

El-Sharkawy MS (2007). Mixing processes and circulation pattern off

Egyptian Mediterranean Coast. Ph.D. Thesis, Oceanographic Department, Faculty of Science, Alexandria University.
Hornea EPW, Lodera JW, Naimeb CE, Oakeyb NS (1996). Turbulence dissipation rates and nitrate supply in the upper water column on Georges Bank. Deep Sea Research part II. Top. Stud. Oceanogr. 4(37-8): 1683-1712.
Johnson GC (1996). Stress on the Mediterranean outflow plume: Part II. Turbulent dissipation and shear measurements. J. Phys. Oceanogr. 24(10): 2084-2092.
Kelly AK (2005). Comparison of Modeled and observed sea surface temperature in the Eastern Mediterranean sea. Program of Analysis and Modeling in the Aegean and Eastern Mediterranean Sea. Program period May 2004 – April 2006.
Kobayashia S, Simpsona JH, Fujiwarab T, Porburghc KJ (2006). Tidal stirring and its impact on water column stability and property distribution in a semi-enclosed shelf sea (Seta Island, Japan). Continental Shelf Res., 26(11): 1295-1306.
MEDAR Group, MEDATLAS/2002 database (2002): Mediterranean and Black Sea database of temperature, salinity and biochemical parameters (4 CDs, IFREMER.
MacPhee-Shaw E (2006). Boundary-Interior Exchange: Reviewing the idea that internal wave mixing enhances lateral dispersion near continental margins. Deep Sea Res., Part II, Top. Stud. Oceanogr. 53(1-2): 42-59.
Mohamed EEE, El- Sharkawy MS, Saad NN , Anwar H (1999). A study of circulation, water masses, and Mixing processes in the southern Mediterranean off the Egyptian Coast during Autumn. J. KAU: Mar. Sci., 10: 3–15.
Molinari RL, Swallow J, Festa JF (1986). Evolution of the near surface thermal structure in the Western Indian Ocean during FGGE, 1979. J. Mar. Res., 44: 739-762.
Morcos SA, Hassan HM (1976). The water masses and circulation in the South-Eastern Mediterranean. Acta Adriatica, 18:12.
Munka W, Wunschb C (1998). Abyssal Recipes II: Energetics of tidal and wind mixing. Deep Sea Res. Part I, Oceanogr. Res. Papers 45(12): 1977-2010.
Peters H (1999). Spatial and temporal variability of mixing in anestuary. J. Mar. Res., 57: 805-845.
Proudman J (1953). Dynamical oceanography. John Wiley & Sons, inc.
Pond S, Pickard G (1983). Introductory oceanography. Pergamon Press
Robert HS (2005). Introduction of Physical Oceanography, Chapter 8, Copyright 1997 – 2005.
Rossa T, Lueckb R (2005). Estimating turbulent dissipation rates from acoustic backscatter. Deep Sea Res. Part I: Oceanogr. Res. Papers 52(12): 2353-2365.
Sharaf El-Din SH (1964). The circulation and mixing processes in the river Mersey and the Irish Sea. Ph. D. Thesis, Liverpool University.
Sparnocchia S, Gasparini GP, Astraldi M, Borghini M, Pistek P (1999). Dynamics and mixing of the Eastern Mediterranean outflow in the Tyrrhenian basin. J. Marine Syst., 20(1-4): 301-317.
Nabil NS, El-Sharkawy MS (2009). Evaluation of Some Dynamical Parameters at the Central Red Sea during Early Summer. J. KAU: Mar. Sci., Vol. 21 (under press).
Yoshida J, Neil SO (1996). Characterization of vertical mixing at a tidal-front on Georges Bank. Deep Sea Research Part II: Top. Stud. Oceanogr., 43(7-8): 1713-1744.